

Synthesis of 3D flower-like cobalt sulfide hierachitecture for high-performance electrochemical energy storage

Shuo Zhang · Chuang Li · Huaqing Xiao ·
Guijuan Wei · Yan Zhou · Zhaojie Wang · Jun Zhang ·
Changhua An

Received: 24 February 2017 / Accepted: 23 May 2017 / Published online: 5 June 2017
© Springer Science+Business Media Dordrecht 2017

Abstract In this work, rationally designed 3D cobalt sulfide nanoflowers (3D CoS NF) were prepared by a facile one-step solvothermal method. The 3D CoS NFs were assembled from low dimensional building blocks with thin 2D nanoflakes with an average thickness of 19 nm (between 1 and 100 nm). SEM and TEM images revealed that the flower-like hierachitecture consisted with an average diameter of 12 μm . XRD data indicated that the as-prepared sample had a pure hexagonal CoS crystal structure. Such 3D CoS NF was applied for fast-charge storage device which delivered a specific capacity of 669 C g⁻¹ at a current density of 1 A g⁻¹. By assembling the 3D CoS NF into an asymmetric

supercapacitor (ASC), the device showed 129.0 C g⁻¹ capacity and long cycle stability (85.7% retention after 3000 cycles).

Keywords Cobalt sulfide · Supercapacitor · Nanoflower · Solvothermal · Fast-charge storage

Introduction

The demand on developing new energy conversion and storage devices has merged the increasing concerns about global warming and air pollutions (Dunn et al. 2011). Besides, fast-charging devices are extremely desired for modern lives, such as mobile phones, laptops, and cameras. Electrochemical capacitors, also known as supercapacitors (SCs), have been demonstrated to be a great candidate to fill in the gap between batteries and conventional capacitors, which can deliver fast charging–discharging rate and high power delivery or uptake (Kötz and Carlen 2000; Miller and Simon 2008). Modern supercapacitors are categorized based on the charge storage mechanisms: electrical double-layer capacitors (EDLCs), pseudocapacitors, and hybrid capacitors (Simon and Gogotsi 2008). Nevertheless, all of the three types of supercapacitors rely on the activated surface areas of the electrode materials to provide either increased ion adsorption/desorption or enlarged active sites.

In order to provide enlarged surface area of the electrode materials, 3D materials were vastly reported for different electrode materials such as porous carbon

Electronic supplementary material The online version of this article (doi:10.1007/s11051-017-3905-8) contains supplementary material, which is available to authorized users.

S. Zhang · C. Li · H. Xiao · G. Wei · Y. Zhou · Z. Wang ·
C. An
College of Science, China University of Petroleum (East China),
66 Changjiang West Road, Qingdao Economic Development
Zone, Qingdao 266580 Shandong, People's Republic of China

Y. Zhou (✉) · Z. Wang · J. Zhang
State Key Laboratory of Heavy Oil Processing, China University
of Petroleum (East China), 66 Changjiang West Road, Qingdao
Economic Development Zone, Qingdao 266580 Shandong,
People's Republic of China
e-mail: yanzhou@upc.edu.cn

C. An (✉)
College of Chemistry and Chemical Engineering, Tianjin
University of Technology, 300384 Tianjin, People's Republic of
China
e-mail: anchh@upc.edu.cn

materials (Yang et al. 2014, 2016, 2017a, b), transition metal oxides (Wu et al. 2010; Xia et al. 2011), hydroxides (Li et al. 2013; Wang et al. 2010a), and chalcogenides (Tu et al. 2016; Wang et al. 2016). Among them, cobalt sulfide is considered to be an excellent electrode material for fast-charging devices (Chen et al. 2016; Lin et al. 2015; Tang et al. 2015). Nanosheets constructed 3D flower-shaped nanostructures that exhibit decent capacitance in supercapacitor applications, thanks to the enlarged surface areas and active sites (He et al. 2015; Luo et al. 2014a). The morphologies of CoS can be greatly influenced by the selection of reaction solvent. Different morphologies can be obtained by different solvents such as ethanol (Dong et al. 2011; Wang et al. 2010b, 2011), ethylene glycol (Gu 2013; Liu et al. 2015), and diethylenetriamine (Hu et al. 2010). In addition, Bao et al. suggested that the addition of ethanol in water solution would decrease the surface energy of CoS nanoparticles, as well as the interaction of hydrogen bonds between small CoS nanoparticles, which can lead the formation of flower-like CoS nanowires (Bao et al. 2008). Therefore, the addition of ethanol in ethylenediamine is believed to assist the formation of CoS with 3D flower-like morphology. Besides, single-phase CoS is highly desired since the well-defined morphologies, thus leads to a uniform charge storage mechanism. Consequently, single-phase nanoflakes' constructed flower-shaped CoS is ideal for enhanced performance in supercapacitors.

In this work, novel 3D flower-like CoS (3D CoS NF) architectures were prepared by one-step solvothermal process using ethanol and ethylenediamine as solvents. The 3D CoS NFs were assembled from 2D CoS nanoflakes. This nanostructure is believed to enhance the effective interaction between active materials and electrolyte and shorten the diffusion length of charge carriers in energy storage applications. The hexagonal flower-shaped CoS showed excellent specific capacity with up to 669 C g^{-1} at 1 A g^{-1} charge–discharge current density and 129.0 C g^{-1} capacity in an asymmetric supercapacitor device.

Experimental

Chemicals

Cobalt chloride hexahydrate ($\text{CoCl}_2 \cdot 6\text{H}_2\text{O}$), thiourea, absolute ethanol, ethylenediamine (En), potassium

hydroxide (KOH), carbon black, and polytetrafluorethylene (PTFE) were purchased from Sinopharm Chemical Reagent Co. Ltd. The activated carbon (YP-50) was purchased from Kuraray Co. Ltd. (Japan). All the materials were analytical reagent grade and used as received without any further purification.

CoS preparation

In a typical procedure, $\text{CoCl}_2 \cdot 6\text{H}_2\text{O}$ (0.8 mmol) and $\text{CH}_4\text{N}_2\text{S}$ (1.6 mmol) were dissolved in 24 mL absolute ethanol and a transparent blue solution was formed after vigorous agitation for 30 min. Then, 16 mL En was added to this blue solution with stirring for 5 min, and brown suspension was observed. Then, the reaction solution with final volume of 40 mL was obtained. The mixture suspension was transferred into a Teflon-lined autoclave (50 mL) immediately and heated at $200 \text{ }^\circ\text{C}$ for 12 h, and then cooled to room temperature. The as-prepared products were washed three times with deionized water and ethanol, respectively, and then dried in a vacuum oven at $60 \text{ }^\circ\text{C}$ for 10 h. For comparison, the CoS nanoflakes were prepared using the same synthetic procedure, but only 40 mL of En was used as the solvent. The CoS synthesized using a binary solution of ethanol and En and En only is designated as 3D CoS NF and CoS.

Structural characterization

The crystalline structures of the samples were confirmed by powder X-ray diffraction (XRD) using a Philips X'Pert diffractometer with $\text{Cu K}\alpha$ radiation ($\lambda = 0.15418 \text{ nm}$). Scanning electron microscopy (SEM) was conducted with a Hitachi S-4800 field emission scanning electronic microscopy (FE-SEM). Transmission electron microscopy (TEM) and high-resolution transmission electron microscope (HR-TEM) analysis were obtained on a JEM-2100UHR transmission electron microscope (JEOL, Japan) operated at 200 kV. Fourier transform-infrared (FTIR) spectra were measured by using a Thermo Nicolet FTIR spectrometer (NEXUS, USA). N_2 adsorption–desorption experiments were carried out on a ChemBET 3000 (Quantachrome, USA) instrument at 77 K. Brunauer–Emmett–Teller (BET) method was used to calculate the surface areas, and the Barrett–Joyner–Halenda (BJH) method was used to evaluate the pore size distributions of the samples.

Electrochemical measurements

For electrochemical measurements, the working electrode was prepared by mixing the electroactive material (3D CoS NF or CoS), carbon black, and PTFE binder in a weight ratio of 80:15:5. A small amount of absolute ethanol was added to the mixture to achieve a homogeneous slurry. The slurry was pressed onto a Ni foam (1.5 cm × 2.0 cm) under 10 MPa by using a tablet press and dried in a vacuum oven at 60 °C for 12 h. Electrochemical measurements were conducted using a CHI 660E electrochemical workstation in an aqueous KOH electrolyte (2.0 M) with a three-electrode setup. The nickel foam served as working electrode; a Pt foil served as the counter electrode, and a Hg/HgO electrode served as the reference electrode.

The electrochemical performances of supercapacitors were evaluated by characterizing their cyclic voltammetry (CV), galvanostatic charge/discharge (GCD), and electrochemical impedance spectroscopy (EIS). The CV was conducted in a potential interval between 0 and 0.7 V vs. Hg/HgO at scan rates ranging from 5 to 100 mV s⁻¹. The GCD tests were performed within a potential range of 0 to 0.55 V vs. Hg/HgO at charge-discharge current densities ranging from 1 to 50 A g⁻¹. The EIS measurements were conducted using an AC voltage with 5 mV amplitude in a frequency range of 0.01 Hz–100 kHz at open circuit potential, and the resultant spectra were simulated using Zview software. To obtain the double-layer capacitance (Cdl), the CV was conducted in a potential interval between -0.4 and -0.3 V vs. Hg/HgO, and the cathodic and anodic current densities increased as the scan rate varied from 20 to 300 mV s⁻¹. All the electrochemical measurements were performed at room temperature.

The specific capacity was calculated according to the GCD curve using Eq. 1:

$$C_m = \frac{I \times \Delta t}{m} \quad (1)$$

where C_m (C g⁻¹) is the specific capacity, I (A) represents the discharge current, Δt (s) represents the discharge time, and m (g) designates the mass of active materials. Since the non-linear relationship between potential and time at a constant current, specific capacity is more reasonable for evaluating the charge storage performance instead of specific capacitance.

To fabricate the asymmetric supercapacitor (ASC), an activated carbon (AC) electrode was prepared by

mixing 95 wt% of activated carbon and 5 wt% of PTFE (as a binder) and then spread on to a Ni foam (1.5 cm × 2.0 cm) as the negative electrode. The subsequent processing of negative electrode and the preparation of the positive electrode were the same as that of the working electrode in a three-electrode system. The electrochemical performances of the ASC devices were performed on a CHI 660E electrochemical workstation in an aqueous KOH electrolyte (2.0 M).

In order to obtain a charge balance between the two electrodes, $q^+ = q^-$ should be satisfied (q^+ is the positive charge and q^- is the negative charge). The mass of activated carbon was calculated using Eq. 2:

$$C_m^+ \times m^+ = C_m^- \times m^- \quad (2)$$

where C_m (C g⁻¹) is the specific capacity and m (g) designates the mass of electrode materials.

Equations 3 and 4 were used to calculate the energy density and power density of the ASC devices, respectively:

$$E = C_m \Delta V / 2 \quad (3)$$

$$P = E / \Delta t \quad (4)$$

where C_m (C g⁻¹) is the specific capacity of the ASC, ΔV (V) is the voltage window of the ASC, E (Wh kg⁻¹) is the energy density, and P (W kg⁻¹) is the power density.

Results and discussion

The crystal structure of 3D CoS NF and pristine CoS was firstly evaluated by XRD as shown in Fig. 1a. All the diffraction peaks can be indexed to hexagonal CoS (JCPDS No. 03-065-3418) with the (100), (101), (102), and (110) crystal planes consisted with the diffraction peaks of 30.63°, 35.30°, 46.93°, and 54.44°, respectively. No other diffraction peaks can be observed in the XRD patterns, indicating the high purity of as-prepared CoS. Figure 1b shows a typical SEM image of pristine CoS; it is clear that the pristine CoS was the aggregation of CoS flakes. In comparison, the 3D CoS NF shown in Fig. 1c indicates flower-like structure. The average diameter of the flowers was found to be 12 μm, suggesting reasonable size distribution for the nanoflakes. The average thickness of each 3D CoS NF nanoflake was

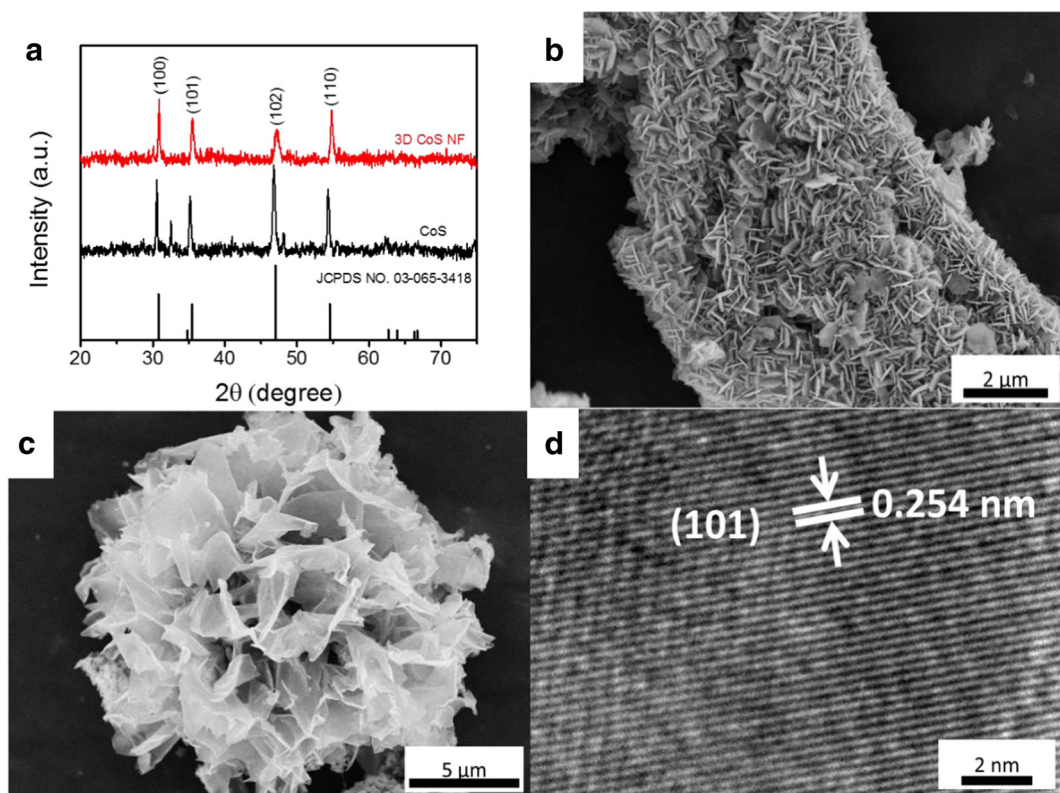


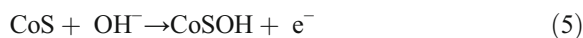
Fig. 1 **a** XRD patterns of 3D CoS NF and CoS. **b** SEM image of pristine CoS. **c** SEM image of 3D CoS NF. **d** HRTEM image of 3D CoS NF

found to be 19 nm (Fig. S1). The HR-TEM image (Fig. 1d) shows the lattice fringe of the CoS NF with an interplanar spacing of 0.254 nm which is consisted with the (101) lattice plane. Figure S3 shows the FTIR spectra of CoS and 3D CoS NF, in which the samples show similar bands. Two peaks at about 3340 and 3212 cm^{-1} are attributed to the N–H symmetric and asymmetrical stretching vibration, and the bands centered at 1630, 1081, and 776 cm^{-1} correspond to the N–H bending vibration, C–N stretching vibration, and N–H out-of-plane bending vibration, respectively, demonstrating the existence of the ethylenediamine in the surface of CoS and 3D CoS NF.

The N_2 adsorption–desorption isotherms of 3D CoS NF shown in Fig. S4a indicate specific area of only 12.7 $\text{m}^2 \text{g}^{-1}$, and the pore size distribution was evaluated by BJH method, and the pore size distribution is narrow and centered at 3.7 nm (Fig. S4b). To estimate the effective electrode surface area, the double-layer capacitance (C_{dl}) is obtained by CV at non-Faradaic potentials (between -0.3 and -0.4 V vs. Hg/HgO) at variable scan rates (Fig. S4c, S4d and S4e). The C_{dl} of 5.5 mF cm^{-2} for 3D CoS NF electrode is much larger than that of CoS

(3.7 mF cm^{-2}). Since C_{dl} is directly related to the surface area of the electrode materials, the high C_{dl} value for 3D CoS NF indicates enlarged surface area compared with CoS.

The electrochemical properties of 3D CoS NF and CoS were examined by CV as shown in Fig. 2a. The two oxidation peaks and the corresponding reverse peaks can be attributed to the oxidation of CoS to CoSOH and CoSOH to CoSO, separately, for both 3D CoS NF and pristine CoS (Luo et al. 2014b):



In order to obtain the insights of electrochemical oxidation process of CoS, CV at variable scan rates was measured and shown in Fig. 2b. The corresponding plots of peak potential against logarithm of scan rate revealed the quasi-reversible electron transfer process, and the Randles–Sveinik plots suggest that the process is diffusion controlled, which is due to the diffusion of

OH^- onto the electrochemical active materials (Fig. S2). Subsequently, the comparison of electrochemical performance of 3D CoS NF and CoS toward charge storage was evaluated by GCD process (Fig. 2c). The specific capacity achieved a maximum of 669 C g^{-1} for 3D CoS NF and 442 C g^{-1} for CoS at a current density of 1 A g^{-1} . These results suggest that rational design of CoS structure is important toward the enhancement in high-performance charge storage devices. Figure 2d shows that there is a decrement of specific capacity with the increasing current density for 3D CoS NF, which is due to insufficient hydroxyl group-coupled Faradaic redox reaction time under high discharge rates (Shi et al. 2015; Zhang et al. 2015). This process is then limited by the diffusion rate of ions within the electrochemical active materials. However, even at a current density of 50 A g^{-1} , the CoS electrode retained 66.6% to its original capacity with 445 C g^{-1} (Fig. 2e). Furthermore, in order to investigate the detailed electrochemical characteristics of CoS, EIS measurements were performed. The resultant Nyquist plots are shown in Fig. 2f. The EIS spectra exhibited a depressed arc in the high-frequency range, followed by a straight line in the low-frequency range. The enlargement of the EIS

spectra in the high-frequency region and the equivalent circuit proposed to fit the spectra are shown as the insets of Fig. 2f, in which R_s is the bulk solution resistance, R_{ct} is the Faradaic interfacial charge transfer resistance, CPE represents the constant phase element accounting for a double-layer capacitance, and W is the Warburg impedance. The semicircle in the high-frequency range is associated with microstructural properties of the CoS electrode and corresponds to R_{ct} with ca. 0.3Ω , indicating high conductivity and thus leads to a superior Faradaic redox reaction kinetics.

Since the above discussions were based on a three-electrode system, it was necessary to evaluate the performance of CoS in a more realistic asymmetric device, which was based on a two-electrode system. The ASC device was assembled by taking AC as the negative electrode and 3D CoS NF or pristine CoS as the positive electrode in 2 M KOH electrolyte. The potential window of the device was chosen by taking the CV measurements separately for 3D CoS NF and AC as shown in Fig. 3a. The rectangular shape was retained between 0 and $-1.0 \text{ V vs. Hg/HgO}$ for AC, and oxidation and reverse peaks were observed from 0 V up to $+0.6 \text{ V vs. Hg/HgO}$ for the Faradaic potential range of 3D CoS

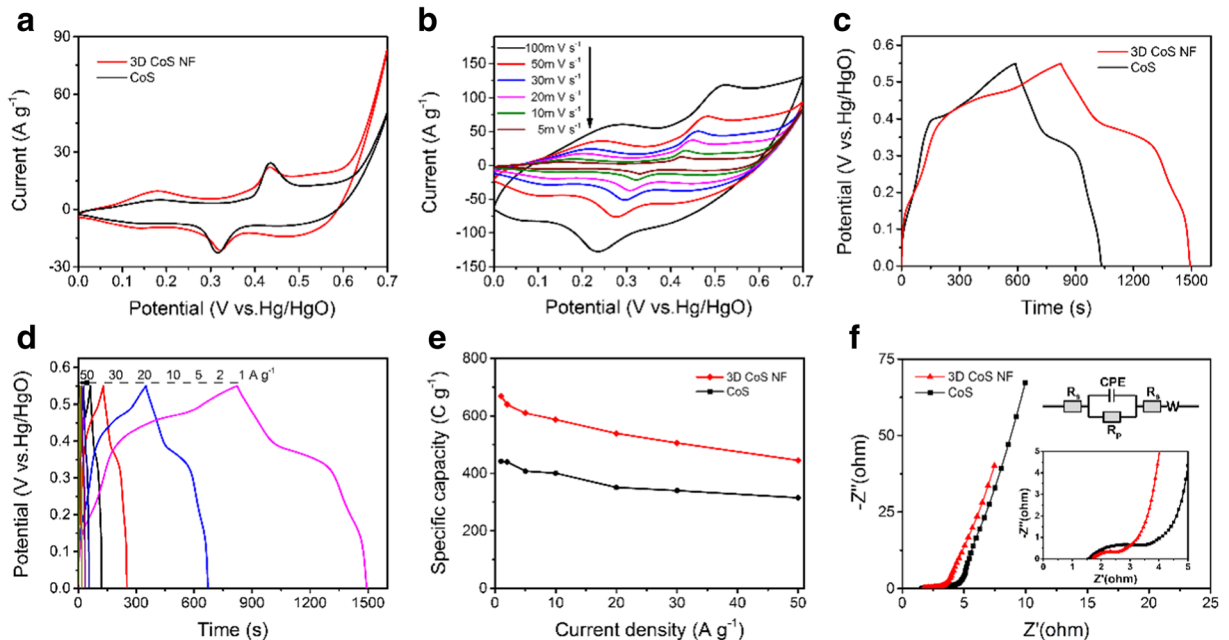


Fig. 2 a Cyclic voltammograms of 3D CoS NF and CoS in 2 M KOH at 10 mV s^{-1} . b Cyclic voltammograms of 3D CoS NF in 2 M KOH at variable scan rates. c Charge-discharge curves for 3D CoS NF and CoS at 1 A g^{-1} . d Charge-discharge curves for 3D CoS NF at different charge current densities. e The trend of

decrement of specific capacity of 3D CoS NF and CoS with increasing charging current density. f Nyquist plots of 3D CoS NF and CoS electrode. In a, c, e, and f, red represents 3D CoS NF, and black represents CoS

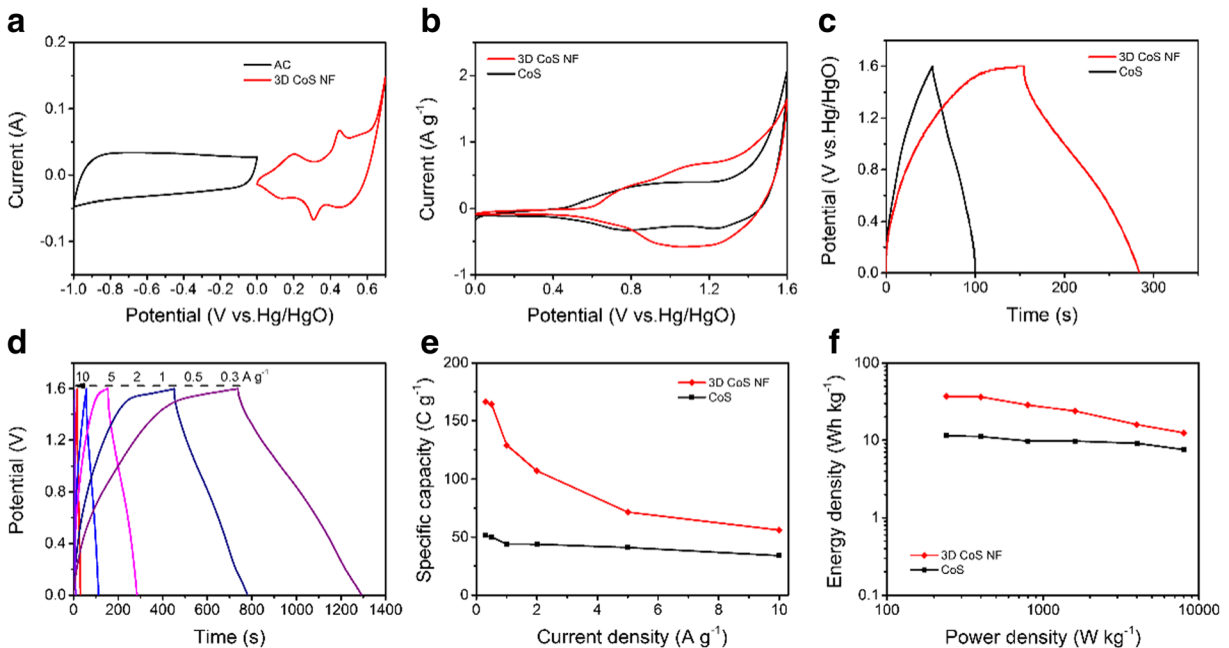


Fig. 3 **a** Cyclic voltammograms of AC and 3D CoS NF electrodes performed in a three-electrode configuration in 2 M KOH electrolyte at 20 mV s^{-1} . **b** Cyclic voltammograms of 3D CoS NF//AC and CoS//AC in 2 M KOH at 10 mV s^{-1} . **c** Charge-discharge curves for 3D CoS NF//AC and CoS//AC at 1 A g^{-1} . **d**

Charge-discharge curves for 3D CoS NF//AC ASC at different charge current densities. **e** The trend of decrement of specific capacity of 3D CoS NF//AC and CoS//AC with increasing charging current density. **f** Ragone plots related to energy and power densities of the ASC

NF, before the electrolysis of water occurs. Therefore, 1.6 V was chosen as the overall potential that applied on both sides of the asymmetric device.

The electrochemical performance of the assembled ASC was evaluated by CV and GCD analysis. As shown in Fig. 3b, the area enclosed by the CV curve of the 3D CoS NF//AC ASC with a voltage window of 0–1.6 V is apparently larger than that of the CoS//AC ASC. This result was also confirmed by the GCD measurements. As shown in Fig. 3c, at a current density of 1 A g^{-1} , the specific capacity of 3D CoS NF//AC and CoS//AC is 129.0 and 43.9 C g^{-1} , respectively, which indicates the better electrochemical behavior of the 3D CoS NF//AC device. Figure 3d illustrates the charge-discharge curves of the 3D CoS NF//AC ASC at different current densities, while Fig. 3e displays the trend of decrement of specific capacity of 3D CoS NF//AC and CoS//AC with increasing charging current density. The specific capacity decreases with the increase of the current density, which is caused by non-ideal diffusion conditions which are similar to those in three-electrode system (Rakhi et al. 2014). In addition, the Ragone plots related to energy and power densities of the 3D CoS NF//AC and CoS//AC ASC are shown in Fig. 3f. The 3D CoS NF//AC ASC shows the

energy density from 37.0 to 12.4 Wh kg^{-1} at the power density from 0.24 to 8 kW kg^{-1} .

Cycling stability is crucial for practical applications. 3D CoS NF//AC and CoS//AC ASC were tested with a voltage of 1.6 V at a current density of 10 A g^{-1} . As shown in Fig. 4, both 3D CoS NF//AC and CoS//AC display long cycle lives, and the 3D CoS NF//AC ASC

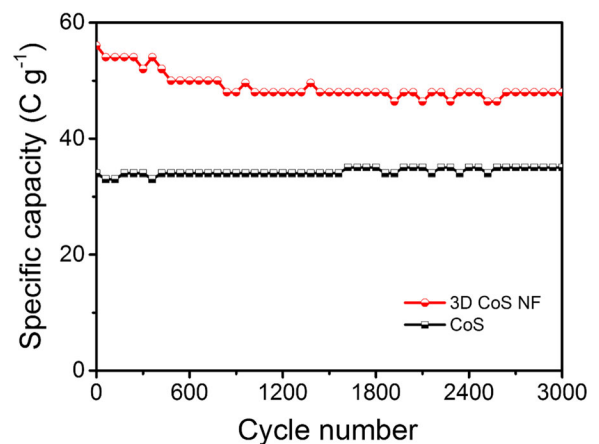


Fig. 4 Cycling performance of the 3D CoS NF//AC (red) and CoS//AC ASC (black) with a voltage of 1.6 V at a current density of 10 A g^{-1}

shows capacitance retention of 85.7% after 3000 cycles at a constant current density of 10 A g^{-1} . It is worth noting that there was a significant decrease in specific capacity of 3D CoS NF||AC ASC. This may be due to the morphological distortion of the 3D structure of CoS NF. Even though, these results suggest that 3D CoS NF can be applied as a decent anode material toward commercial ASC.

Conclusion

In conclusion, we demonstrated a rational synthetic design to fabricate 3D flower-like CoS hierarchitectures by a one-step binary solution solvothermal process. Compared with pristine CoS that was synthesized using ethylenediamine, the solution of ethanol and ethylenediamine mixture assisted successfully toward the fabrication of the 3D CoS NF. This rationally designed hierarchical architecture not only facilitates the infiltration of electrolyte but also provides more active sites. Such CoS electrode delivered a specific capacity of 669 C g^{-1} at a current density of 1 A g^{-1} . By assembling the 3D CoS NF into an ASC, the device showed 129.0 C g^{-1} capacity and long cycle stability. This synthetic strategy can be valuable toward controlled manipulation of CoS structures, such leading to enhanced performances.

Acknowledgements The authors thank the financial supports provided by National Natural Science Foundation of China (No. 21471160), the Fundamental Research Funds for the Central Universities (16CX05014A, 16CX05016A), and the Taishan Scholar Program of Shandong Province.

Compliance with ethical standards

Funding This study was funded by National Natural Science Foundation of China (No. 21471160), the Fundamental Research Funds for the Central Universities (16CX05014A, 16CX05016A), and the Taishan Scholar Program of Shandong Province.

Conflict of interest The authors declare that they have no conflict of interest.

References

- Bao S-J, Li CM, Guo C-X, Qiao Y (2008) Biomolecule-assisted synthesis of cobalt sulfide nanowires for application in supercapacitors. *J Power Sources* 180:676–681. doi:10.1016/j.jpowsour.2008.01.085
- Chen MH, Zhang JW, Xia XH, Qi ML, Yin JH, Chen QG (2016) Construction of cobalt sulfide/nickel core-branch arrays and their application as advanced electrodes for electrochemical energy storage. *Electrochim Acta* 195:184–191. doi:10.1016/j.electacta.2016.02.143
- Dong W et al (2011) Hydrothermal synthesis and structure evolution of hierarchical cobalt sulfide nanostructures. *Dalton Trans* 40:243–248
- Dunn B, Kamath H, Tarascon J-M (2011) Electrical energy storage for the grid: a battery of choices. *Science* 334:928
- Gu Y (2013) Graphene-wrapped CoS nanoparticles for high-capacity lithium-ion storage. *ACS Appl Mater Interfaces* 5: 801
- He D, Wu D, Gao J, Wu X, Zeng X, Ding W (2015) Flower-like CoS with nanostructures as a new cathode-active material for rechargeable magnesium batteries. *J Power Sources* 294: 643–649. doi:10.1016/j.jpowsour.2015.06.127
- Hu QR, Wang SL, Zhang Y, Tang WH (2010) Synthesis of cobalt sulfide nanostructures by a facile solvothermal growth process. *J Alloys Compd* 491:707–711
- Kötz R, Carlen M (2000) Principles and applications of electrochemical capacitors. *Electrochim Acta* 45:2483–2498. doi:10.1016/S0013-4686(00)00354-6
- Li M, Xu S, Liu T, Wang F, Yang P, Wang L, Chu PK (2013) Electrochemically-deposited nanostructured Co(OH)₂ flakes on three-dimensional ordered nickel/silicon microchannel plates for miniature supercapacitors. *J Mater Chem a* 1: 532–540. doi:10.1039/C2TA00160H
- Lin TW, Hsiao MC, Chou SW, Shen HH, Lin JY (2015) Glucose-assisted synthesis of nickel-cobalt sulfide/carbon nanotube composites as efficient cathode materials for hybrid supercapacitors. *J Electrochem Soc* 162:A1493–A1499. doi:10.1149/2.0511508jes
- Liu S et al (2015) Facile synthesis of novel networked ultralong cobalt sulfide nanotubes and its application in supercapacitors. *ACS Appl Mater Interfaces* 7: 25568–25573
- Luo F, Li J, Yuan H, Xiao D (2014a) Rapid synthesis of three-dimensional flower-like cobalt sulfide hierarchitectures by microwave assisted heating method for high-performance supercapacitors. *Electrochim Acta* 123:183–189. doi:10.1016/j.electacta.2014.01.009
- Miller JR, Simon P (2008) Electrochemical capacitors for energy management. *Science* 321:651
- Rakhi RB, Alhebshi NA, Anjum DH, Alshareef HN (2014) Nanostructured cobalt sulfide-on-fiber with tunable morphology as electrodes for asymmetric hybrid supercapacitors. *J Mater Chem A* 2:16190–16198. doi:10.1039/c4ta03341h
- Shi J, Li X, He G, Zhang L, Li M (2015) Electrodeposition of high-capacitance 3D CoS/graphene nanosheets on nickel foam for high-performance aqueous asymmetric supercapacitors. *J Mater Chem A* 3:20619–20626. doi:10.1039/c5ta04464b
- Simon P, Gogotsi Y (2008) Materials for electrochemical capacitors. *Nat Mater* 7:845–854
- Tang YF et al (2015) A highly electronic conductive cobalt nickel sulphide dendrite/quasispherical nanocomposite for a supercapacitor electrode with ultrahigh areal specific capacitance. *J Power Sources* 295:314–322. doi:10.1016/j.jpowsour.2015.07.035
- Tu CC, Lin LY, Xiao BC, Chen YS (2016) Highly efficient supercapacitor electrode with two-dimensional tungsten

- disulfide and reduced graphene oxide hybrid nanosheets. *J Power Sources* 320:78–85. doi:10.1016/j.jpowsour.2016.04.083
- Wang H, Casalongue HS, Liang Y, Dai H (2010a) Ni(OH)₂ nanoplates grown on graphene as advanced electrochemical pseudocapacitor materials. *J Am Chem Soc* 132:7472–7477. doi:10.1021/ja102267j
- Wang MQ, Fei HF, Zhang P, Yin LW (2016) Hierarchically layered MoS₂/Mn₃O₄ hybrid architectures for electrochemical supercapacitors with enhanced performance. *Electrochim Acta* 209:389–398. doi:10.1016/j.electacta.2016.05.078
- Wang Q et al (2010b) Novel flower-like CoS architectures: one-pot synthesis and electrochemical properties. *J Mater Chem* 21:327–329
- Wang Q et al (2011) Facile synthesis and superior supercapacitor performances of three-dimensional cobalt sulfide architectures. *CrystEngComm* 13:6960–6963
- Wu M-S, Wang M-J, Jow J-J (2010) Fabrication of porous nickel oxide film with open macropores by electrophoresis and electrodeposition for electrochemical capacitors. *J Power Sources* 195:3950–3955. doi:10.1016/j.jpowsour.2009.12.136
- Xia X-h, Tu J-p, Mai Y-j, Wang X-l, Gu C-d, Zhao X (2011) Self-supported hydrothermal synthesized hollow Co₃O₄ nanowire arrays with high supercapacitor capacitance. *J Mater Chem* 21:9319–9325. doi:10.1039/C1JM10946D
- Yang X, Li C, Chen Y (2017a) Hierarchical porous carbon with ultrahigh surface area from corn leaf for high-performance supercapacitors application. *J Phys D Appl Phys* 50:055501. doi:10.1088/1361-6463/50/5/055501
- Yang X, Li C, Fu R (2016) Nitrogen-enriched carbon with extremely high mesoporosity and tunable mesopore size for high-performance supercapacitors. *J Power Sources* 319:66–72. doi:10.1016/j.jpowsour.2016.04.037
- Yang X, Yu J, Zhang W, Zhang G (2017b) Mesopore-dominant wormhole-like carbon with high supercapacitive performance in organic electrolyte. *RSC Adv* 7:15096–15101. doi:10.1039/c7ra00446j
- Yang X, Zhang G, Zhong M, Wu D, Fu R (2014) Ammonia-assisted semicarbonization: a simple method to introduce micropores without damaging a 3D mesoporous carbon nanonetwork structure. *Langmuir ACS J Surf Colloids* 30:9183–9189. doi:10.1021/la5008846
- Zhang Y, Li L, Su H, Huang W, Dong X (2015) Binary metal oxide: advanced energy storage materials in supercapacitors. *J Mater Chem a* 3:43–59. doi:10.1039/c4ta04996a